

Journal of Biomedical Optics

SPIDigitalLibrary.org/jbo

Quantitative characterization of articular cartilage using Mueller matrix imaging and multiphoton microscopy

Pål Gunnar Ellingsen
Magnus Borstad Lilledahl
Lars Martin Sandvik Aas
Catharina de Lange Davies
Morten Kildemo

Quantitative characterization of articular cartilage using Mueller matrix imaging and multiphoton microscopy

Pål Gunnar Ellingsen, Magnus Borstad Lilledahl, Lars Martin Sandvik Aas, Catharina de Lange Davies, and Morten Kildemo
Norwegian University of Science and Technology, Department of Physics, Faculty of Natural Sciences and Technology,
Institutt for Fysikk, 7491 Trondheim, Norway

Abstract. The collagen meshwork in articular cartilage of chicken knee is characterized using Mueller matrix imaging and multiphoton microscopy. Direction and degree of dispersion of the collagen fibers in the superficial layer are found using a Fourier transform image-analysis technique of the second-harmonic generated image. Mueller matrix images are used to acquire structural data from the intermediate layer of articular cartilage where the collagen fibers are too small to be resolved by optical microscopy, providing a powerful multimodal measurement technique. Furthermore, we show that Mueller matrix imaging provides more information about the tissue compared to standard polarization microscopy. The combination of these techniques can find use in improved diagnosis of diseases in articular cartilage, improved histopathology, and additional information for accurate biomechanical modeling of cartilage. © 2011 Society of Photo-Optical Instrumentation Engineers (SPIE). [DOI: 10.1117/1.3643721]

Keywords: Mueller matrix imaging; multiphoton microscopy; collagen; cartilage.

Paper 11303R received Jan. 15, 2011; revised manuscript received Aug. 18, 2011; accepted for publication Sep. 6, 2011; published online Oct. 26, 2011.

1 Introduction

Articular cartilage covers and protects the bones in joints, and its integrity is essential for normal function. It imparts two important properties to a joint. First, it provides a low-friction surface for smooth articulation of the joint; second, it provides a cushioning layer to distribute loads and protect the underlying bone. The structure of articular cartilage is typically divided into three distinct morphological zones: (i) The superficial layer with a dense collagen network and the collagen fibers oriented primarily tangential to the articulating surface, (ii) the intermediate layer, where the fibers are more randomly distributed, and (iii) the radial layer, where the fibers are oriented perpendicular to the bone surface. The collagen fibers are cross-linked with proteoglycans in a fluid-saturated gel of glycosaminoglycans and proteoglycans. Scattered throughout the cartilage are chondrocytes that reside in lacunae and are responsible for the formation of new cartilage.¹

Osteoarthritis is a disease in articular cartilage symptomized by pain and reduced joint function, affected by a variety of factors (genetic, traumatic, age, excessive loading).² It is the leading cause of disability in the U.S. and will likely see an increased incidence in the future due to an aging and more obese population.³ Osteoarthritis is characterized by structural changes in the cartilage, accompanied by a loss of proper function. The loss of function will lead to changed loading conditions in the knee and, therefore, further changes in the microscopic structure. In order to predict the outcome of this biological cascade, it is necessary to have methods to characterize the current tissue structure. Osteoarthritis is usually diagnosed based on clinical findings, sometimes with the addition of radiographic

imaging. However, in a significant fraction of symptomatic patients, no radiographic changes are found.⁴ Magnetic resonance imaging may be used for further stratification, but the association between clinical symptoms and findings from images is not always strong.⁵ Therefore, a more detailed investigation using novel imaging techniques, is necessary to enhance diagnosis.

Bright-field light microscopy of haematoxylin-eosin-stained sections is the standard method to assess the microscopic structure of cartilage, even though it is not possible to see the structure of the collagen network. Polarization microscopy is sometimes used but can only provide qualitative information on the direction of collagen fibers due to the complex nature of the polarization properties of tissue. Novel methods to study the microscopic structure of cartilage will provide more details on the current pathological status and perhaps differentiate between conditions that cannot be distinguished with standard techniques.

Multiphoton microscopy (MPM) is a nonlinear optical process used to acquire images of biological specimens.⁶ Because of the nonlinearity of the signals, the technique is intrinsically confocal (no need for confocal optics), and many biological molecules exhibit specific intrinsic nonlinear signatures such that no staining is required. The second-harmonic generation (SHG) signal can be used to image the collagen type II fibers present in cartilage.^{7,8} *In vivo* imaging is possible and yields high-resolution, three dimensional images.⁹ *In vivo* MPM would be a valuable complementary technique to standard arthroscopy. Methods have been developed to generate quantitative measures of the structure of the collagen fabric¹⁰ and its optical properties.¹¹ The drawback of MPM is that high-resolution imaging of macroscopic volumes is time consuming. Furthermore, in the intermediate and radial layers, the collagen fibers are below the resolution limit of optical microscopy, such that individual fibers cannot be resolved.

Address all correspondence to: Morten Kildemo, Norwegian University of a Science and Technology, Department of Physics, Faculty of Natural Sciences and Technology, 7491 Trondheim, Norway; Tel: +0047 73593211; E-mail: morten.kildemo@ntnu.no.

Mueller matrix imaging (MMI) provides a complementary technique to MPM and extracts the full Mueller matrix for every pixel in the image of a sample.¹² Because the resolution is adjustable (but usually worse than MPM by a factor of around 10), and camera-based imaging is used instead of point scanning, larger areas are scanned faster compared to MPM. Because MMI also is an optical technique, it cannot resolve the small collagen fibers in the middle layer. However, the advantage of MMI is that it is based on the rich polarization information contained in the full Mueller matrix, such that the directionality of the fibers may be derived, as well as the optical rotation and depolarization of the sample, by using forward polar decomposition.^{13,14} The use of decomposed Mueller matrix measurements to characterize tissue phantoms and biological samples has been described,^{15,16} but to our knowledge never on samples of cartilage. Compared to other polarimetric imaging systems that only measure some of the components of the Mueller matrix^{17–19} and require significant prior knowledge of the sample and the desired measurements, the Mueller matrix imaging system is much more flexible, enabling the characterization of more complex and unexplored samples with the possibility to fully characterize the polarization properties of the sample. Here, we show that the combination of MPM and MMI provide more detailed information about the articular cartilage structure compared to conventional methods and potentially a better understanding of the progression of osteoarthritis.

2 Materials and Methods

2.1 Materials

The medial femoral condyle of chicken cartilage ($n = 2$) was cut in 100- μm -thick sections to a depth of 2 mm using a vibratome (Leica VT-1000). After sectioning, the samples were transferred to microscope slides and a cover glass placed on top. The edges were sealed with Vaseline to avoid dehydration. Sections were cut in the transversal plane. The sections were kept at 4°C between measurements.

2.2 Multiphoton Microscopy

The MPM images were acquired using a commercial system (Zeiss LSM 510), equipped with a Ti:sapphire laser pumped by a 5-W solid state laser (Coherent Mira and Verdi, respectively). The Ti:sapphire laser was tuned to 800 nm for excitation of the SHG signal. A dichroic short-pass filter at 650 nm was used to collect the backscattered light. A second dichroic at 475 nm and a bandpass filter at 390–425 nm were used to separate the SHG from the fluorescence. All images were acquired in the epi configuration.

Images were acquired with a 10 \times , 0.6 numerical aperture (NA) objective. For samples larger than the field of view, several images were juxtaposed automatically using the microscopy control system. Images were acquired at four to eight different depths, with an interval of 10 μm , depending on the quality of the signal in the deeper sections.

On the basis of an image-analysis algorithm described in detail elsewhere,¹⁰ we derived the primary direction and anisotropy of the fibers at every pixel in the image. Briefly, the algorithm calculates the two-dimensional discrete Fourier transform of a small subframe around a given pixel. Typically, the strongest Fourier components will tend to lie on a line perpendicular to

the fibers in the image. The direction of this line was found by minimizing the sum of angles, weighted by the Fourier power spectrum relative to this line. The anisotropy is extracted as a measure of how close the strongest frequency components are clustered around this line.

2.3 Mueller Matrix Imaging

The near-infrared Mueller matrix imaging (NIR MMI) system used here is described in greater detail elsewhere.¹² Note that the light source used here is the 980-nm laser diode and that the numerical aperture of the system is 0.04. It uses two ferroelectric liquid crystals (FLCs) together with a polarizer and two wave plates to generate four orthogonal Stokes vectors in what is known as a polarization-state generator (PSG), which then are used to probe the sample. After passing through the sample, the resulting polarization-state is analyzed by a polarization state analyzer (PSA), consisting of the same components as the PSG, in reverse order. Sixteen intensity images are acquired using different settings of the PSG and PSA. The Mueller matrix \mathbf{M} is then calculated from the configurations of the PSG and PSA using the eigenvalue calibration method.²⁰ Repeating this for every pixel in the images results in a Mueller matrix image, \mathbf{M}_{im} . The Mueller matrix is normalized, meaning that all of the elements in the matrix is divided by the M_{11} element.

The measured \mathbf{M} is decomposed into depolarization, (\mathbf{M}_{Δ}), retardation, (\mathbf{M}_{R}), and diattenuation, (\mathbf{M}_{D}), matrices using forward polar decomposition, $\mathbf{M} = \mathbf{M}_{\Delta}\mathbf{M}_{\text{R}}\mathbf{M}_{\text{D}}$, first described by Lu and Chipman¹³ and applied by Manhas et al.¹⁴ to tissue characterization.

From \mathbf{M}_{R} , it is further possible to find the linear retardance, direction of the slow axis (perpendicular to the fast axis), and the optical rotation (see Manhas et al.¹⁴). We assume that the collagen fibers can be modeled using the Bruggeman effective medium theory,²¹ and thus assign the slow optical axis to the long axis of the fibers.

3 Results

3.1 Multiphoton Microscopy

SHG images of the superficial layer show a distinct collagen structure, which is illustrated in Fig. 1(a). By employing the direction analysis method described in Sec. 2.2, we derived the primary direction and degree of anisotropy of the fibers, which is shown in Figure 1(b). The direction is coded according to color using the provided legend and the anisotropy is mapped to the intensity of the color. Figure 2(a) shows a sample where both the superficial and intermediate layers can be seen. The center region, which belongs to the superficial zone, exhibits clear fibrillar structure, whereas in the intermediate layer, shown in the lower right part of Fig. 2(a), no collagen fibers can be discerned. Only the lacunae can be seen as dark voids, embedded in a smooth SHG signal. Figure 2(b) shows that the analysis picks up the direction in the superficial region but that in the intermediate layer where no structure can be discerned, the anisotropy is very low, corresponding to low intensity in the color image.

3.2 Mueller Matrix Imaging

MMI images were acquired from the same samples as imaged with MPM. The MMI images were first Cloude filtered²² and

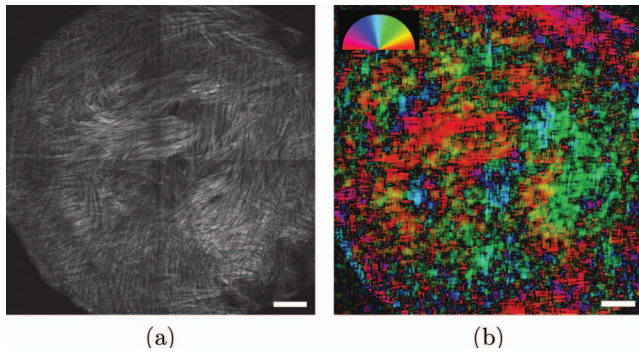


Fig. 1 (a) SHG intensity image of a transverse section of cartilage in the superficial layer ($100\ \mu\text{m}$ below the surface), where the collagen fibers are clearly visible. This image is the result of four images tiled together. (b) Result of the directional analysis. The calculated direction of the fibers is color coded according to the semicircle legend. The intensity of the color has been scaled to the calculated anisotropy value. Scale bar is $200\ \mu\text{m}$.

then decomposed using the forward polar decomposition described in Sec. 2.3. An example of the full Mueller matrix for a cartilage sample is illustrated in Fig. 3. The M_{11} element has been substituted by the intensity image, because this element would be equal to 1 as a result of the normalization. The values of the diattenuation matrix \mathbf{M}_D were found to be very small and are not included here.

After the decomposition, the direction of the slow axis is found from the retardance matrix \mathbf{M}_R .¹⁴ The corresponding image of the directions is illustrated in Fig. 4. Because the long axis of the collagen fibers corresponds to the optical slow axis, the directional image shows the collagen fiber direction and can be compared to the MPM image of the same sample, as shown in Fig. 5.

The forward polar decomposition enables in addition to the direction of the slow axis, the calculation of the amount of double refraction in the sample known as the linear retardance (which is seen in Fig. 6), the amount of left or right circular polarization induced by the sample, known as the optical rotation (shown in Fig. 7), and the depolarization index (as seen in Fig. 8). The

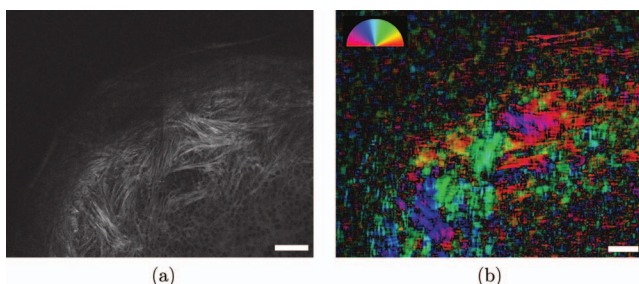


Fig. 2 (a) SHG intensity image of a transverse section of cartilage from slightly below the superficial layer ($500\ \mu\text{m}$ below the surface). The central part of the image belongs to the superficial region, and here, the fibers are clearly visible. The lower right part belongs to the intermediate layer. No clear structure of fibers can be seen in this region, only the lacunae are distinguishable as dark voids. (b) Result of directional analysis. The calculated direction of the fibers is color coded according to the semicircle legend. The intensity of the color has been scaled by the calculated anisotropy value. In the intermediate layer, only a weak random direction is picked up. Scale bar is $200\ \mu\text{m}$.

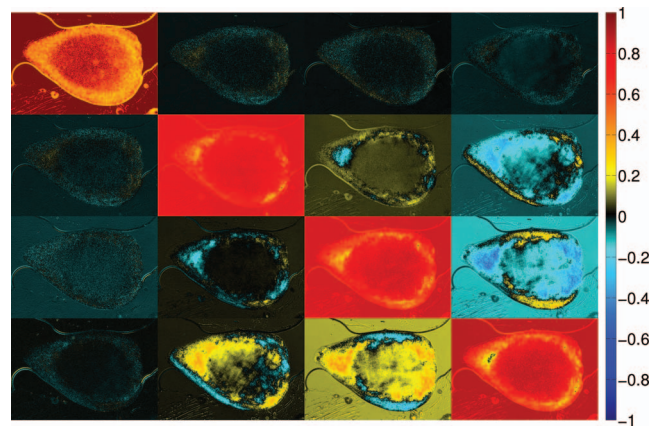


Fig. 3 Full Cloude-filtered Mueller matrix image for a sample of cartilage, from a transversal section at a depth of $500\ \mu\text{m}$, with the intensity image overlaid the M_{11} element. The central dark area in M_{11} is the intermediate layer, and the surrounding bright area is the superficial layer.

depolarization index shows how much of the incoming polarized light is converted into partially polarized light.

The intermediate zone of the cartilage (center of Figs. 4 and 6) exhibits more variation and features in the MMI images compared to what can be seen in the MPM images. In this intermediate zone, the direction and retardance images show regions with differing structure.

4 Discussion

The Mueller matrix was decomposed into three polarization properties of which only the retardation and depolarization were used directly in this study. The retardance (circular, linear, and direction of fast axis) will, in terms of effective medium theory, yield results from features smaller than the resolution in the image. The latter property is useful, because it can be used to characterize collagen fibers from the intermediate and radial zone of the cartilage, where the collagen fibrils are below the resolution limit of MPM.

Because the collagen fibers have a higher refractive index than the surrounding medium,²³ they will have the slow axis

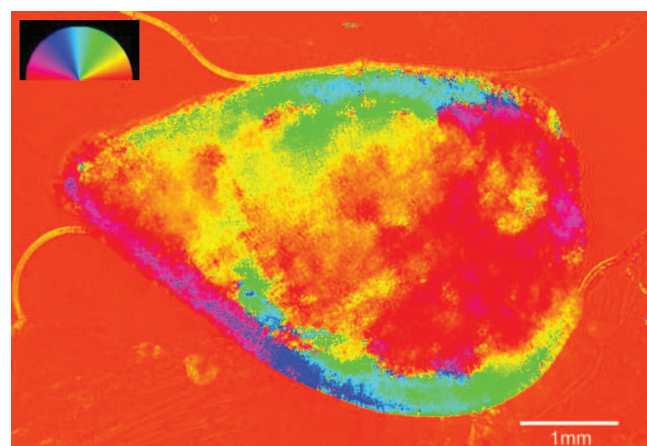


Fig. 4 Visualization of the direction of the slow axis found from \mathbf{M}_R .

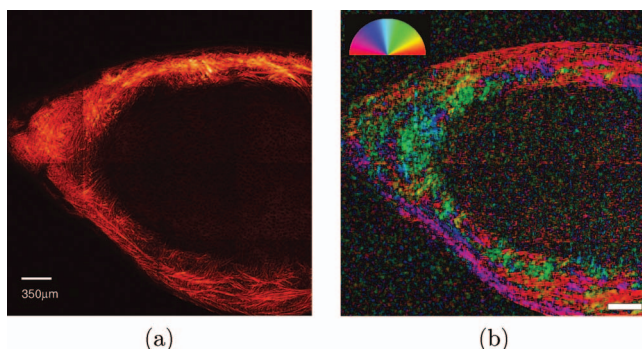


Fig. 5 (a) SHG images from the same area as the MMI images and (b) calculated directions of image in (a).

along the long axis. The difference in the refractive index of the slow and fast axes can be calculated using the simple linear dispersion relation for a birefringent medium

$$\Delta n = \frac{\lambda \delta}{2\pi L},$$

where λ is the wavelength (here, 980 nm), δ the linear retardance (in radians), and L the thickness of the sample (here, 100 μm). Using a representative value of $\delta = 50$ deg for the edges of the sample, as seen in Fig. 6, and $\delta = 15$ deg for the intermediate region, results in an apparent birefringence $\Delta n = 1.4 \times 10^{-3}$ for the edges, similar to previously reported values,²⁴ and $\Delta n = 0.4 \times 10^{-3}$ from intermediate regions. As Fig 6 shows, there are large differences in the linear retardance across the sample, resulting in large differences in Δn , such that care should be taken when reporting birefringence measurements of collagen in turbid media.

The slow axis found from the decomposed Mueller matrix is the projection of the three-dimensional slow axis into the imaging plane. In addition, since directions found from the Mueller matrix measurement are from a volume, the directions seen in Fig. 4, will be an average of the collagen fibers through the sample as opposed to the MPM images, which are acquired at a certain depth (Fig. 5). Even when taking the latter into consideration, the directions in the sample correspond well to the direction in the corresponding MPM image, indicating that the

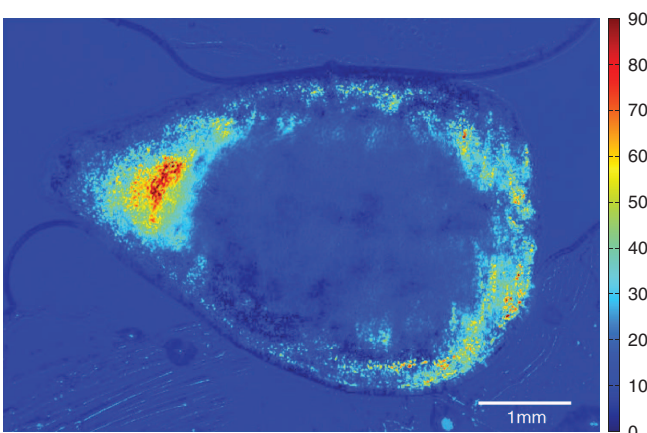


Fig. 6 Retardance image, showing the absolute value of the linear retardance. Color bar is in degrees.

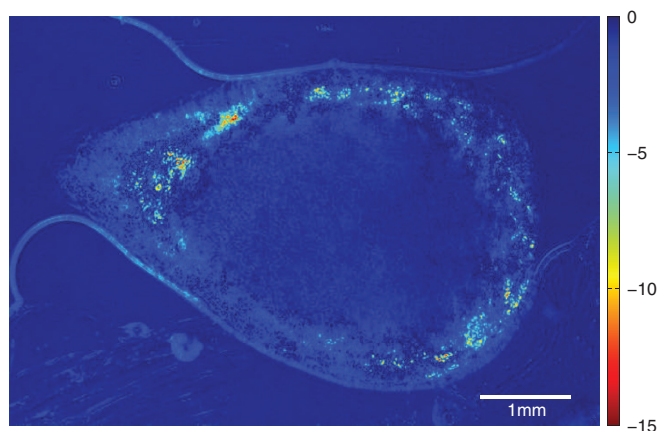


Fig. 7 Optical rotation in degrees.

direction of the collagen fibers are mostly homogeneous through the sections. However, when characterizing the samples using MPM some variation in the direction with respect to the depth was observed, which would result in an intermediate direction in the MMI image and correspondingly different calculated values for the directional parameter.

In the intermediate layer (center of Fig. 6), where the MPM images cannot resolve individual collagen fibrils that are smaller than the imaging resolution limit, the MMI directional image shows structure variations and, thus, the ability to characterize the subresolution structures in this area of cartilage.

The collagen fibers in the cartilage scatter the incoming light, contributing to the depolarization (see Fig. 8). The depolarization will increase with the density and size of the collagen fibers, and could thus be useful for extracting more information about the collagen structure. By comparing the depolarization image (shown in Fig. 8) to the retardance image (shown in Fig. 6), one can see that the areas with a high depolarization index are mostly the same areas as the ones with high retardance, indicating a higher concentration or larger size of the collagen fibers, resulting in the higher depolarization. The reason the retardance is small in some areas of high depolarization could be attributed

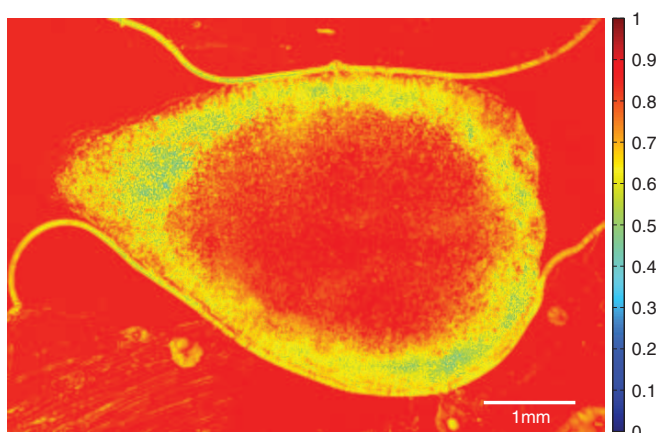


Fig. 8 Depolarization index, where 1 is fully polarized and 0 fully depolarized.

Table 1 Specific rotation for hyaluronic acid (HA), keratane sulfate (KS), and chondroitin sulfate (CS) in a water solution (Ref. 28). In addition, the specific rotation of collagen in 0.5M CaCl₂ is given (Ref. 27). The temperature at which the specific rotation is measured is given, when given in the source. The concentration of the chemical compounds in human femoral head cartilage from ages 3 to 19 are also given (Ref. 29). Total wet volume of tissue per unit weight of collagen (d_c^{-1}) is 4.96 ± 0.041 ml/g (Ref. 29).

Chemical substance	Specific rotation $[\alpha]_{589}$	Wet tissue weight percentage w
HA	-68.2 deg at 27°C	0.16
KS	4.5 deg	0.83 ± 0.095
CS type A	-25 deg	2.86 ± 0.10
Collagen	-360 deg at 8°C	18.5 ± 1.4

to the collagen fibers in that area being aligned at an angle to the image plane, reducing the measured linear retardance.

An interesting observation is that the optical rotation (see Fig. 7) appears large compared to commonly reported values from solution. However, such large values may be justified by considering the triple helix²⁵ structure of the collagen together with proteoglycans. The left-handed collagen helix will induce optical rotation to the incoming polarized light. The amount of induced optical rotation is dependent on the orientation of the collagen fiber, with little contribution from out-of-plane fibers. Cartilage consists of proteoglycans, which contain²⁶ hyaluronic acid (HA), keratane sulfate (KS), and chondroitin sulfate (CS), all of which are optical active. The optical activity of these components are given in Table 1, together with their concentrations in femoral head cartilage. On the basis of these values, the expected optical rotation from a 100- μ m-thick solution of cartilage is calculated using

$$\phi = [\alpha_c]_{583} L d, \quad (1)$$

where ϕ is the expected optical rotation, $[\alpha_c]_{583}$ the specific rotation in Table 1 for the given compound, L the thickness of the sample in decimeter (here, 10^{-3} dm), and d the density in (grams per milliliter), given here by $d = d_c w_s / w_c$, where d_c is the collagen density, w_s the substance weight percentage, and w_c the collagen weight percentage. Using (1) and values from Table 1 gives an optical rotation due to proteoglycans of -8.6×10^{-4} deg, and due to collagen of -0.07 deg at 583 nm, assuming that a 0.5 M CaCl₂ solution has the same optical rotation as water. The proteoglycan contribution to the optical rotation is thus negligible. The measurements of the optical rotation here were done at 980 nm, which is expected to give lower optical rotation due to the two-term Drude equation.²⁷ The optical rotation of the collagen fibers depends on their orientation. Hence, one would expect the ordered collagen fibers in the cartilage to have a higher optical rotation compared to randomly ordered collagen fibers in solution. This corresponds well to the observed values of optical rotation. Figure 7 shows structural variation across the image plane, believed to be caused by changes in the fibril direction relative to the image plane. However the variation in signal across the sample is different

compared to the retardance and depolarization images, indicating that additional information is stored in this image.

The comparison between the direction found from the MPM images and from the MMI images showed that they overall agreed quite well. Discrepancies could be seen toward the edges and at some isolated interior regions. Toward the edges, the Fourier analysis technique used in the MPM analysis will exhibit some artifacts as it picks up the edge of the sample as a strong frequency component (interpreted as a fiber) running tangential to the edge. If the fibers run perpendicularly to the edge, then this will be picked up by MMI and large discrepancies are expected. Other sources of discrepancies could be due to small collagen fibers not resolved by MPM and/or changes in the collagen direction through the sample (MPM could not image completely through the thickness of the sample). The tiling of the microscope images to create images of larger regions is evident in Figs. 1(a) and 2(a), which is due to uneven excitation over the imaging plane, probably due to movement of the beam at the back aperture of the objective. However, it appears that the transition between images is quite well filtered out during image analysis.

MMI will be unable to differentiate between collagen fibers running parallel to the sample surface and fibers that are at an angle to the surface. One way to distinguish these two cases would be to rotate the sample in the beam such that the Mueller matrix is extracted with the collagen fibers rotated at different angles to the incoming beams. By having enough different directions, it should be possible to extract a three-dimensional average direction of the fibers.

The structure of the collagen fibers as seen in the MPM images could be useful in the diagnosis and assessment of osteoarthritis. In this study, the MMI was performed in transmission mode; however the technique can also be applied in reflection mode, which would make it applicable for *in vivo* use. MMI can also be used in conjunction with high NA objectives to achieve even higher resolution images of the polarization properties. In the current setting, however, it is perhaps its ability to image large regions relatively fast that is its main advantage. Histopathology is another field where MMI could be very valuable. Its ability to generate more detailed polarization properties could make it valuable for better assessing the structure of diseased cartilage in histopathology studies. For example, the depolarization index and differences in linear and circular retardation are not picked up by regular polarization microscopes. The detailed structure that is possible to extract with these two imaging techniques could also have important applications in the study of the biomechanics of cartilage.

5 Conclusion

By applying an image-analysis technique based on the Fourier transform on the MPM images, we were able to quantify the direction of the fibers in the superficial layer. Combining this with Mueller matrix imaging proved to be a powerful combination, allowing for the extraction of directional parameters from the intermediate layer. The structure in the intermediate layer is usually assumed to be isotropic, but the retardance images clearly show that there is structural inhomogeneities in the connective tissue in these areas as well. In conclusion, the combination of

MMI and MPM provides a powerful technique in the study of osteoarthritis and other cartilage diseases.

Acknowledgments

We acknowledge Linh Hoang, at the Department of pathology, Children and Women's Health at NTNU, for help in preparing the cartilage samples.

References

1. W. C. Mow, W. Y. Gu, and F. H. Chen, *Structure and Function of Articular cartilage and Meniscus*, 3rd ed., pp. 181–258, Lippincott, Williams and Wilkins, Philadelphia (2005).
2. D. J. Hunter and D. T. Felson, "Osteoarthritis," *BMJ* **332**(7542), 639–642 (2006).
3. "National health interview survey," Tech. Rep., Center for Disease Control and Prevention (2009).
4. M. B. Kinds, P. M. J. Welsing, E. P. Vignon, J. W. J. Bijlsma, M. A. Viergever, A. C. A. Marijnissen, and F. P. J. G. Lafeber, "A systematic review of the association between radiographic and clinical osteoarthritis of hip and knee," *Osteoarth Cartilage* **19**(7), 768–778 (2011).
5. E. Yusuf, M. C. Kortekaas, I. Watt, T. W. J. Huizinga, and M. Kloppenburg, "Do knee abnormalities visualised on mri explain knee pain in knee osteoarthritis? a systematic review," *Ann. Rheum. Dis.* **70**(1), 60–67 (2011).
6. W. Denk, "Two-photon laser scanning fluorescence microscopy," *Science* **248**(4951), 73–76 (1990).
7. A. T. Yeh, M. J. Hammer-Wilson, D. C. Van Sickle, H. P. Benton, A. Zoumi, B. J. Tromberg, and G. M. Peavy, "Nonlinear optical microscopy of articular cartilage," *Osteoarth Cartilage* **13**(4), 345–352 (2005).
8. J. C. Mansfield, C. P. Winlove, J. Moger, and S. J. Matcher, "Collagen fiber arrangement in normal and diseased cartilage studied by polarization sensitive nonlinear microscopy," *J. Biomed. Opt.* **13**(4), 044020 (2008).
9. M. J. Levene, D. A. Dombek, K. A. Kasischke, R. P. Molloy, and W. W. Webb, "In vivo multiphoton microscopy of deep brain tissue," *J. Neurophysiol.* **91**(4), 1908–1912 (2004).
10. M. B. Lilledahl, D. M. Pierce, T. Ricken, G. A. Holzapfel, and C. d. L. Davies, "Structural analysis of articular cartilage using multiphoton microscopy: input for biomechanical modelling," *IEEE Trans. Med. Imaging* (in press).
11. A. Erikson, J. Ortegren, T. Hompland, C. de Lange Davies, and M. Lindgren, "Quantification of the second-order nonlinear susceptibility of collagen I using a laser scanning microscope," *J. Biomed. Opt.* **12**(4), 044002 (2007).
12. L. M. S. Aas, P. G. Ellingsen, and M. Kildemo, "Near infra-red Mueller matrix imaging system and application to retardance imaging of strain," *Thin Solid Films* **519**, 2737–2741 (2011).
13. S. Y. Lu and R. A. Chipman, "Interpretation of Mueller matrices based on polar decomposition," *J. Opt. Soc. Am. A* **13**(5), 1106–1113 (1996).
14. S. Manhas, M. K. Swami, P. Buddhiwant, N. Ghosh, P. K. Gupta, and K. Singh, "Mueller matrix approach for determination of optical rotation in chiral turbid media in backscattering geometry," *Opt. Express* **14**(1), 190–202 (2006).
15. N. Ghosh, M. F.G. Wood, and I. A. Vitkin, "Mueller matrix decomposition for extraction of individual polarization parameters from complex turbid media exhibiting multiple scattering, optical activity, and linear birefringence," *J. Biomed. Opt.* **13**(4), 044036 (2008).
16. N. Ghosh, M. F. G. Wood, S. Li, R. D. Weisel, B. C. Wilson, R. Li, and I. A. Vitkin, "Mueller matrix decomposition for polarized light assessment of biological tissues," *J. Biophot.* **2**(3), 145–56 (2009).
17. L.-W. Jin, K. A. Claborn, M. Kurimoto, M. A. Geday, I. Maezawa, F. Sohrawy, M. Estrada, W. Kaminsky, and B. Kahr, "Imaging linear birefringence and dichroism in cerebral amyloid pathologies," *Proc. Natl. Acad. Sci.* **100**, 15294–15298 (2003).
18. M. Shribak and R. Oldenbourg, "Techniques for fast and sensitive measurements of two-dimensional birefringence distributions," *Appl. Opt.* **42**(16), 3009–3017 (2003).
19. W. Kaminsky, L.-W. Jin, S. Powell, I. Maezawa, K. Claborn, C. Branham, and B. Kahr, "Polarimetric imaging of amyloid," *Micron (Oxford, England: 1993)* **37**, 324–338 (2006).
20. E. Compain, S. Poirier, and B. Drevillon, "General and self-consistent method for the calibration of polarization modulators, polarimeters, and mueller-matrix ellipsometers," *App. Opt.* **38**, 3490–3502 (1999).
21. H. G. Tompkins and E. A. Irene, *Handbook of Ellipsometry*, Vol. 1, William Andrew Publishing/Noyes, Norwich, NY (2005).
22. S. R. Cloude, "Conditions for the physical realisability of matrix operations in polarimetry," *Proc. SPIE* **1166**, 177–185 (1989).
23. V. V. Tuchin, L. V. Wang, and D. A. Zimnyakov, *Optical Polarization in Biomedical Applications*, Springer-Verlag, Berlin (2006).
24. N. Ugryumova and S. J. Matcher, "Variable angle-of-incidence polarization-sensitive optical coherence tomography: its use to study the 3D collagen structure of equine articular cartilage," *Proc. SPIE* **6079**, 60792C (2006).
25. B. Brodsky and J. Ramshaw, "The collagen triple-helix structure," *Matrix Biol.* **15**, 545–554 (1997).
26. D. Heinegård and I. Axelsson, "Distribution of keratan sulfate in cartilage proteoglycan," *J. Bio. Chem.* **252**, 1971–1979 (1977).
27. P. H. Vonhippel and K. Y. Wong, "The collagen gelatin phase transition. II. shape of the melting curves and effect of chain length," *Biochemistry* **2**(6), 1399–1413 (1963).
28. Combined Chemical Dictionary Online Version 14.2," Taylor & Francis, Boca Raton, FL (2011).
29. A. Maroudas, M. T. Bayliss, and M. F. Venn, "Further studies on the composition of human femoral head cartilage," *Ann. Rheum. Dis.* **39**(5), 514–523 (1980).